A Two-Qubit Controlled-NOT Gate for Multi-Color Quantum Photonic Systems

Hiva Shahoei, Duncan L. MacFarlane, Mitchell A. Thornton
The Darwin Deason Institute for Cybersecurity
Department of Electrical and Computer Engineering
The Bobby B. Lyle School of Engineering
Southern Methodist University
Dallas, Texas, USA
{hshahoei, dmarcfarlane, mitch}@smu.edu

***Abstract*— We present a conceptual KLM-style implementation of a two-qubit controlled-NOT (CNOT) gate for frequency-encoded (multi-color) photonic qubits. The CNOT operation is constructed through an H–CZ–H decomposition, where programmable frequency-domain Hadamard transformations are implemented using a parallel frequency-mixing architecture. This parallel configuration enables controlled redistribution of probability amplitudes among frequency bins while maintaining scalability and reduced parasitic loss compared to serial architectures. The nonlinearity required for the CZ gate is realized through two-photon interference at a partial beam splitter within an otherwise linear optical system, without requiring auxiliary photons. This approach provides a resource-efficient and scalable framework for frequency-domain quantum logic and multi-color photonic quantum information processing.**

Keywords—Controlled-NOT (CNOT) gate, controlled-phase (CZ) gate, frequency-bin qudits, two-photon interference, post-selection, quantum photonic integrated circuits (QPICs), quantum frequency processing

I. Introduction

Controlled two-qudit gates form the cornerstone of quantum information processing, as they enable the generation of entanglement and, together with arbitrary single-qudit operations, constitute a universal gate set for quantum computation. Among these, the controlled-NOT (CNOT) gate plays a central role, serving as a fundamental building block for quantum algorithms, error correction, and quantum communication protocols. As a result, the physical realization of high-fidelity controlled gates remains a central challenge across all quantum hardware platforms.

Photonic systems offer an attractive platform for quantum information processing due to their low decoherence, ease of manipulation, and natural compatibility with communication networks. However, the absence of strong optical nonlinearities at the single-photon level makes the direct implementation of deterministic two-qudit gates particularly challenging. A seminal breakthrough in this context was provided by the Knill–Laflamme–Milburn (KLM) scheme, which demonstrated that scalable quantum computation is possible using only linear optical elements, single-photon sources, and measurements [1]. KLM showed that effective photon–photon interactions can be created using ancilla photons and measurement-post selection. Fully scalable KLM is experimentally very demanding due to the substantial photon overhead required for ancillary resources, as well as the need for fast, low-loss feed-forward control. To reduce this complexity, a simplified conceptual KLM-style approach has been adopted, where the gate operates solely on the control and target photons and successful events are identified through post-selection rather than active feed-forward architecture. In this framework effective photon–photon interactions are induced through multi-photon interference and post-selection, enabling the realization of controlled operations such as the controlled-phase (CZ) gate, which can be converted into a CNOT gate via local basis transformations on the target qubit. While previous demonstrations of linear-optical CNOT gates primarily relied on polarization or path encoding [2-7], recent advances have highlighted the promise of frequency encoding as a powerful and scalable degree of freedom for photonic quantum information. Frequency-encoded qubits and qudits provide access to a large Hilbert space within a single spatial mode, offering intrinsic stability, compatibility with integrated photonics, and direct interfacing with fiber-based communication systems. Moreover, electro-optic modulation and spectral phase control enable flexible and reconfigurable manipulation of frequency bins using mature telecom technologies.

In this work, we present a linear-optical realization of a CNOT gate for frequency-encoded photonic qubits, inspired by the conceptual-KLM approach using two photon interference and measurement-induced nonlinearity without auxiliary photons. The gate relies solely on the control and target photons, with successful events identified by post-selecting coincident detections corresponding to one photon in each output mode.

II. CNOT gate architecture

Following the standard construction in quantum information, the CNOT operation is obtained from a controlled-phase (CZ) gate by applying Hadamard transformations to the target qubit before and after the phase interaction, H-CZ-H operation. This decomposition allows the gate implementation to focus on realizing the conditional phase shift, while single-qubit Hadamard operations complete the CNOT transformation.

In other words, the CNOT gate is implemented as H–CZ–H acting on the target qubit. In the following sections, we describe our approach for realizing both the Hadamard and the controlled-phase (CZ) operations.

A. Hadamard Gate Implementation

The Hadamard operation on the target qubit is realized using a parallel frequency-domain quantum processor [8, 9]. In this architecture, the input optical state is encoded in discrete frequency bins. A frequency demultiplexer first separates the input frequencies into parallel spatial branches, each corresponding to one frequency bin of the quantum state. Within each branch, electro-optic frequency mixing is performed using phase-modulation structures driven by appropriately programmed multi-tone RF signals. For a d -dimensional quantum state, each RF modulation signal typically contains $(d-1)$ cosine components, each with specified amplitudes and phases. By properly controlling these amplitudes and phases, the modulation redistributes the probability amplitudes among the frequency bins while imposing the required relative phase shifts.

Each branch therefore contributes a programmed portion of the overall unitary transformation, and the processed components are subsequently recombined using a frequency multiplexer to produce the final output state. The architecture described herein scales gracefully to states of higher dimension, has a desirable geometry and footprint when implemented as a quantum photonic integrated circuit (QPIC) cell, and has a preferable overall loss characteristic in comparison to the "quantum Fourier processor" (QFP) architecture as described in [10-12]. For the case of a two-dimensional system (d = 2), the processor implements the Hadamard operation by equally redistributing the probability amplitudes between the two frequency bins with the required relative phase shift. The block diagram of the proposed Hadamard gate implementation is shown in Fig. 1. An input frequency-encoded qubit is first demultiplexed into its constituent frequency bins. The separated components are then processed in parallel by an RF-driven electro-optic modulation stage that performs the required frequency mixing to achieve the desired amplitude redistribution and relative phase shift. The modulated frequency components are then recombined through a multiplexer to produce the Hadamard-transformed output state.

The amplitudes and phases of the RF modulation tones are determined through numerical optimization. The optimization adjusts the amplitudes and phases of the RF tones driving the electro-optic modulation stage to achieve the required redistribution of probability amplitudes and relative phase between the frequency bins. The objective function is defined using the gate fidelity between the obtained transformation and the ideal Hadamard operation. By maximizing this fidelity, the optimization identifies the RF drive parameters that best approximate the desired unitary transformation. Using this approach, a fidelity of 0.9631 is obtained when an MZM configuration is used for the electro-optic modulation stage, while a nested MZM implementation achieves a significantly higher fidelity of 0.9996. This improvement reflects the greater control provided by the nested structure over the generated frequency components and their relative phases. However, this gain in fidelity comes with additional implementation complexity. Compared with a single MZM, the nested MZM generally requires a larger device footprint, introduces more optical loss due to the additional components and splitting/combining stages, and demands more RF control signals and bias settings. Therefore, a practical tradeoff exists between gate fidelity and system complexity, where the nested MZM offers superior performance at the expense of increased hardware requirements.

Fig. 1. Block diagram of the frequency-domain Hadamard gate implemented using a parallel architecture. The input multicolor qubit is demultiplexed into frequency bins, processed in parallel by RF-driven electro-optic modulation stages, and recombined to produce the Hadamard-transformed output state.

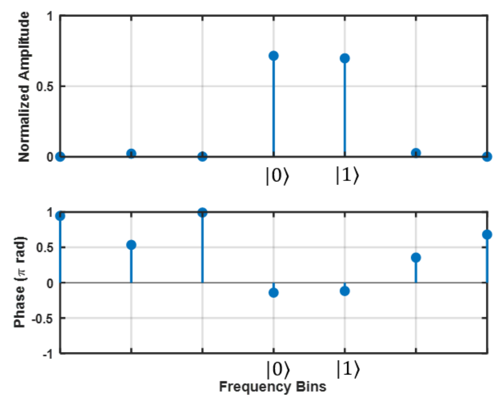

Fig. 2. Normalized amplitudes and phases of the frequency-bin states after frequency mixing for an input state $|0\rangle$. The optimized modulation redistributes the probability amplitudes equally between $|0\rangle$ and $|1\rangle$, producing the superposition state $(|0\rangle + |1\rangle)/\sqrt{2}$. The upper plot shows the normalized amplitudes of the frequency bins, while the lower plot shows the corresponding phases (normalized to π).

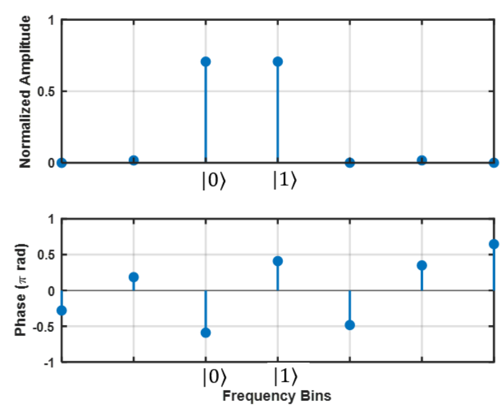

Fig. 3. Normalized amplitudes and phases of the frequency-bin states after frequency mixing for an input state $|1\rangle$. The optimized modulation redistributes the probability amplitudes equally between $|0\rangle$ and $|1\rangle$, producing the state $(|0\rangle - |1\rangle)/\sqrt{2}$. The upper plot shows the normalized amplitudes of the frequency bins, while the lower plot shows the corresponding phases (normalized to π).

Fig. 2 illustrates the normalized amplitudes and phases of the frequency-bin states at the output of the top mixer after optimization of the RF modulation parameters. This case corresponds to an input state in the computational basis $|0\rangle$. The programmed modulation redistributes the probability amplitudes between the two computational frequency bins, producing equal amplitudes in $|0\rangle$ and $|1\rangle$ with zero relative phase. This corresponds to the Hadamard transformation of the input state, where the output becomes a superposition of the two frequency bins. The spectral components outside the computational bins remain negligible, confirming that the mixing process predominantly redistributes the probability amplitudes within the desired frequency bins. Similarly, Fig. 3 illustrates the normalized amplitudes and phases of the frequency-bin states at the output of the lower mixer after optimization of the RF modulation parameters. This case corresponds to an input state in the computational basis $|1\rangle$. The programmed modulation redistributes the probability amplitudes between the two computational frequency bins, producing equal amplitudes in $|0\rangle$ and $|1\rangle$ with a relative phase of π, corresponding to the expected Hadamard transformation of the input state.

B. Controlled-Phase (CZ) Gate Implementation

The controlled-phase (CZ) interaction is implemented using two-photon interference at a partially reflecting beam splitter (PRBS). When two indistinguishable photons arrive simultaneously at the beam splitter inputs, their probability amplitudes interfere coherently. This interference modifies the amplitudes of coincidence and bunching events and enables an effective conditional phase shift in the post-selected two-photon state [13, 14].

A beam splitter with transmission amplitude t and reflection amplitude r is shown in Fig. 4. The modes C and T correspond to the control and target inputs, respectively. The beam splitter transforms the creation operators as, $\hat{C}^\dagger \to t\hat{C}^\dagger + r\hat{T}^\dagger, \hat{T}^\dagger \to t\hat{T}^\dagger - r\hat{C}^\dagger$, with the normalization condition $t^2 + r^2 = 1$ [1, 13]. For an input state with one photon in each mode, $|11\rangle$, the output state becomes $|11\rangle \to (t^2 - r^2)|11\rangle + tr(|20\rangle - |02\rangle)$. The term proportional to $t^2 - r^2$ corresponds to coincidence events, where one photon exits each output port, while the remaining terms correspond to photon bunching, where both photons exit the same port.

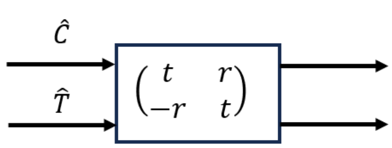

Fig. 4. Partially reflecting beam splitter (PRBS) used to implement the controlled-phase (CZ) interaction. Control (C) and target (T) photons interfere at the beam splitter with transmission t and reflection r. Post-selected coincidence events produce the conditional π-phase shift.

To realize a controlled-phase interaction, a π-phase shift must be applied only when both the control and target photons are present. This requires the coincidence amplitude of the two-photon state to acquire a negative sign relative to the single-photon case. Imposing the condition $t^2 - r^2 = -t^2$, together with $t^2 + r^2 = 1$, yields $t^2 = 1/3, r^2 = 2/3$.

Thus, a beam splitter with transmission $T = 1/3$ and reflection $R = 2/3$ produces the required sign inversion of the two-photon coincidence term. By post-selecting the coincidence detection events, the two-photon component therefore acquires an effective π-phase shift relative to the single-photon terms. This post-selected operation succeeds with probability $1/9$, corresponding to coincidence detection at the output ports.

C. Full CNOT gate Implementation

The complete CNOT gate is realized using the standard decomposition in which Hadamard operations are applied to the target qubit before and after the controlled-phase (CZ) interaction. In this construction, the first Hadamard transforms the target qubit into the superposition basis, enabling the conditional phase shift to be mapped into a conditional bit flip. After the CZ operation applies a π-phase shift to the joint $|11\rangle$ component, the second Hadamard converts this phase shift into the logical CNOT transformation. The overall gate operates probabilistically, and successful operation is identified through post-selection of coincidence events corresponding to one photon in each output mode. The block diagram of the complete H–CZ–H CNOT architecture is shown in Fig. 5. The action of the proposed architecture is verified here. Using frequency-bin encoding, we define, $|0\rangle_C \equiv C_{f1}$, $|1\rangle_C \equiv C_{f2}$, $|0\rangle_T \equiv T_{f1}$, $|1\rangle_T \equiv T_{f2}$. Thus, the most general two-qubit input state can be written as

$$\Psi_{\text{in}} = \alpha\, C_{f1}T_{f1} + \beta\, C_{f1}T_{f2} + \gamma\, C_{f2}T_{f1} + \delta\, C_{f2}T_{f2}.$$

The Hadamard applied to the target frequency bins is

$$H: T_{f1} \to \frac{1}{\sqrt{2}}(T_{f1} + T_{f2}), T_{f2} \to \frac{1}{\sqrt{2}}(T_{f1} - T_{f2}).$$

After the first Hadamard, the state becomes

$$\Psi_1 = \frac{1}{\sqrt{2}}[\alpha C_{f1}(T_{f1} + T_{f2}) + \beta C_{f1}(T_{f1} - T_{f2}) + \gamma C_{f2}(T_{f1} + T_{f2}) + \delta C_{f2}(T_{f1} - T_{f2})].$$

The second stage is the CZ gate, to apply the conditional phase to the appropriate frequency-bin pair, the modes are first demultiplexed into spatial paths. The selected paths interfere at beam splitters with transmission $T = 1/3$ and reflection $R = 2/3$. Additional splitters are included in the other branches so that all computational paths acquire the same amplitude factor $1/3$. The CZ stage therefore introduces only a relative phase on the $|11\rangle$, $C_{f2}T_{f2}$, components:

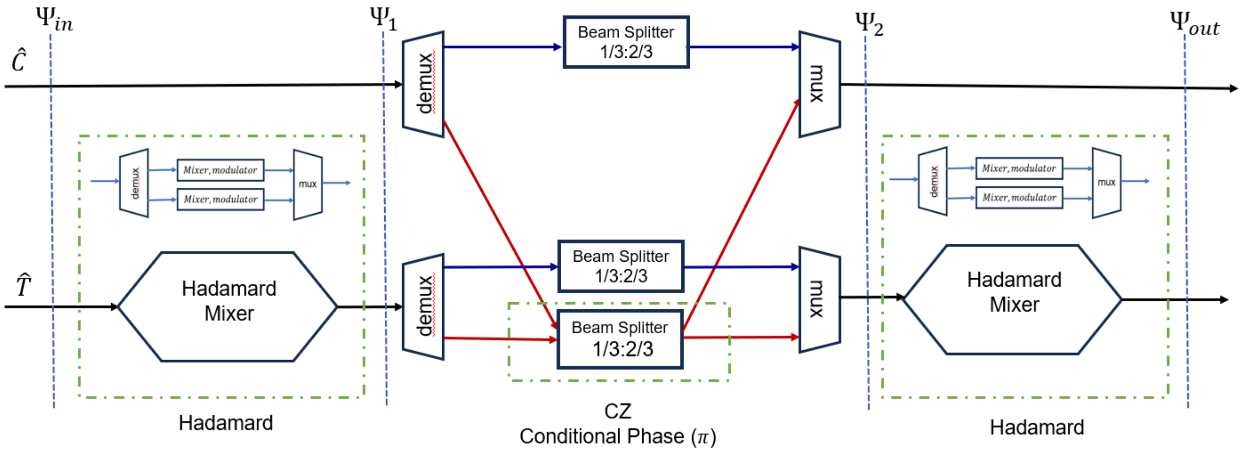

Fig. 5. (a) Block diagram of the proposed H–CZ–H implementation of the CNOT gate. The target qubit undergoes a Hadamard transformation, followed by a controlled-phase (CZ) interaction implemented via two-photon interference, and a final Hadamard operation. Successful gate operation is identified through post-selected coincidence detection.

$$\Psi_2 = \frac{1}{3\sqrt{2}}[\alpha C_{f1}(T_{f1} + T_{f2}) + \beta C_{f1}(T_{f1} - T_{f2}) + \gamma C_{f2}(T_{f1} - T_{f2}) + \delta C_{f2}(T_{f1} + T_{f2})].$$

Applying the second Hadamard mixer on the target yields

$$\Psi_{out} = \frac{1}{3}[\alpha C_{f1}T_{f1} + \beta C_{f1}T_{f2} + \gamma C_{f2}T_{f2} + \delta C_{f2}T_{f1}].$$

Ignoring the common post-selection factor $1/3$, the resulting transformation corresponds to the CNOT operation, $|00\rangle \to |00\rangle$, $|01\rangle \to |01\rangle$, $|10\rangle \to |11\rangle$, $|11\rangle \to |10\rangle$. Thus the target frequency bin flips conditioned on the control being in state C_{f2}.

To illustrate the operation of the proposed architecture, Fig. 6(a–d) shows the evolution of the four computational basis states as they propagate through the circuit. Here, $|f_1\rangle$ and $|f_2\rangle$ denote single-photon states occupying the corresponding frequency bins used to encode the logical qubit states. In each case, the target frequency bin is first transformed by the Hadamard mixer, producing a superposition of f_1 and f_2. The frequency components are then demultiplexed into spatial paths where the selected modes interfere at the $1/3{:}2/3$ beam splitters implementing the CZ operation. Finally, the modes are recombined and a second Hadamard transformation is applied to the target, yielding the corresponding CNOT output state.

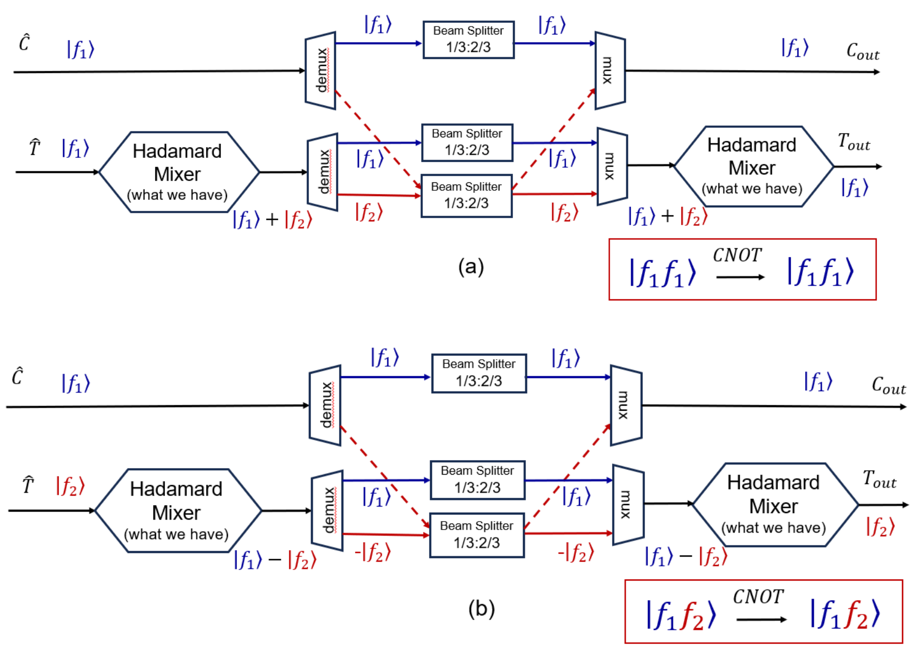

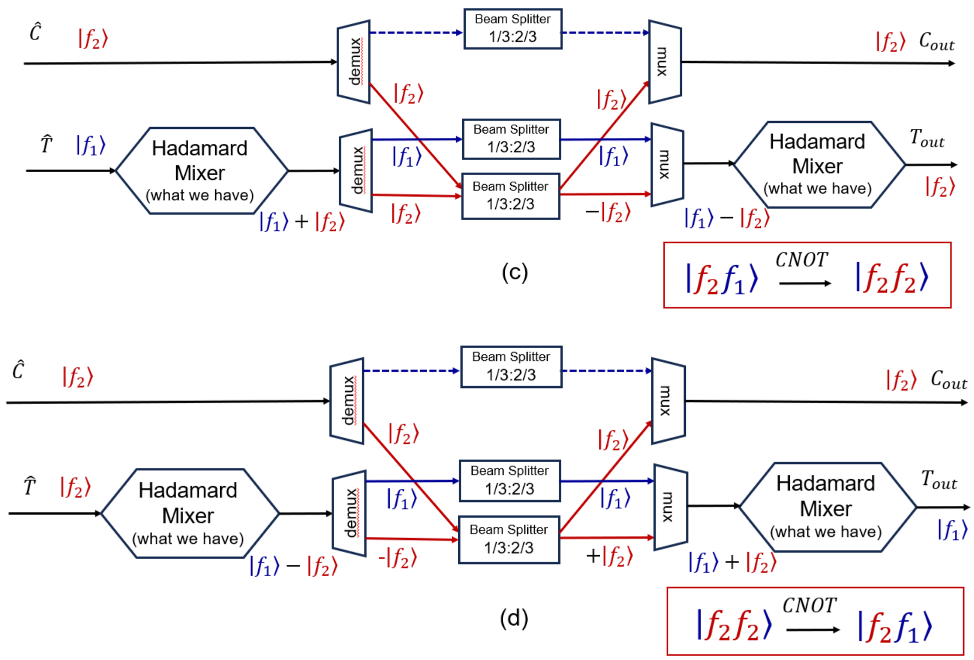

Fig. 6. Evolution of the four computational basis states through the proposed $CNOT$ architecture: (a) $|00\rangle$, (b) $|01\rangle$, (c) $|10\rangle$, and (d) $|11\rangle$. The frequency bins f_1 and f_2 represent the logical qubit states. The target mode first undergoes a Hadamard transformation, the frequency components are demultiplexed to implement the CZ interaction at the $1/3{:}\,2/3$ beam splitters, and the modes are finally recombined before the second Hadamard produces the CNOT output. The coefficients $(1/\sqrt{2}, 1/3)$ are intentionally left out.

III. Conclusion

We have presented a conceptual KLM-style implementation of a two-qubit CNOT gate for frequency-encoded (multi-color) photonic qubits. The approach combines measurement-induced nonlinearity for the controlled-phase (CZ) interaction with programmable frequency-domain Hadamard operations realized using a parallel electro-optic modulator/mixer architecture. By decomposing the CNOT as H–CZ–H on the target qubit, the implementation separates single-qubit frequency mixing from the two-photon interference mechanism that generates the conditional phase shift.

The gate operates probabilistically and is verified through post-selected coincidence detection, eliminating the need for auxiliary photons and active feed-forward control. The parallel frequency-processing architecture provides programmability, scalability to higher-dimensional qudits, and compatibility with photonic integration platforms. This framework offers a flexible and resource-efficient route toward frequency-domain quantum logic and multi-color photonic quantum information processing.

References

[1] E. Knill, R. Laflamme, G. J. Milburn, "A scheme for efficient quantum computation with linear optics," Nature, vol. 409, pp. 46–52, Jan. 2001.

[2] T. C. Ralph, N. K. Langford, T. B. Bell, and A. G. White, "Linear optical controlled-NOT gate in the coincidence basis," *Phys. Rev. A*, vol. 65, no. 6, Art. no. 062324, Dec. 2001.

[3] H. F. Hofmann and S. Takeuchi, "Quantum phase gate for photonic qubits using only beam splitters and postselection," *Phys. Rev. A*, vol. 66, no. 2, Art. no. 024308, Nov. 2001.

[4] J. L. O'Brien, G. J. Pryde, A. G. White, T. C. Ralph, and D. Branning, "Demonstration of an all-optical quantum controlled-NOT gate," *Nature*, vol. 426, no. 6964, pp. 264–267, Nov. 2003.

[5] A. Politi, M. J. Cryan, J. G. Rarity, S. Yu, and J. L. O'Brien, "Silica-on-silicon waveguide quantum circuits," *Science*, vol. 320, no. 5876, pp. 646–649, May 2008.

[6] A. Politi, J. C. F. Matthews, and J. L. O'Brien, "Shor's quantum factoring algorithm on a photonic chip," *Science*, vol. 325, no. 5945, pp. 1221–1221, Sep. 2009.

[7] I. Piasetzky, R. Shnaiderman, and U. Levy, "High-fidelity CNOT gates in photonic integrated circuits using composite segmented directional couplers," *arXiv preprint*, arXiv:2509.25505, 2025.

[8] D. L. MacFarlane, H. Shahoei, R. M. Tuller, C. Shapard, C. Crowson, and M. A. Thornton, "Parallel architecture of a frequency comb qudit quantum processor," *arXiv preprint*, arXiv:2508.15981, 2025.

[9] D. L. MacFarlane, H. Shahoei, R. M. Tuller, C. Shapard, C. Crowson, and M. A. Thornton, "Parallel architecture of a frequency comb qudit quantum processor," *Proc. IEEE Int. Symp. Multiple-Valued Logic (ISMVL)*, 2026.

[10] J. Lukens and P. Lougovski, "Frequency-encoded photonic qubits for scalable quantum information processing," *Optica*, vol. 4, no. 1, pp. 8–16, Jan. 2017.

[11] H. H. Lu, "Electro-optic frequency beam splitters and tritters for high-fidelity photonic quantum information processing," *Phys. Rev. Lett.*, vol. 120, no. 3, Jan. 2018

[12] M. Kues, C. Reimer, J. M. Lukens, et al., "Quantum optical microcombs," *Nature Photonics*, vol. 13, no. 3, pp. 170–179, Mar. 2019.

[13] C. K. Hong, Z. Y. Ou, and L. Mandel, "Measurement of subpicosecond time intervals between two photons by interference," *Phys. Rev. Lett.*, vol. 59, no. 18, pp. 2044–2046, Oct. 1987.

[14] J. L. O'Brien, "Optical quantum computing," *Science*, vol. 318, no. 5856, pp. 1567–1570, Dec. 2007.